





Article

Mixed Matrix Membranes Using Porous Organic Polymers (POPs)—Influence of Textural Properties on CO₂/CH₄ Separation

Laura Matesanz-Niño ^{1,2} , Jorge Moranchel-Pérez ³, Cristina Álvarez ^{1,2} , Ángel E. Lozano ^{1,2,4} 
and Clara Casado-Coterillo ^{3,*} 

- ¹ Department of Applied Macromolecular Chemistry, Instituto de Ciencia y Tecnología de Polímeros, ICTP-CSIC, Juan de la Cierva 3, E-28006 Madrid, Spain; laura.matesanz@ictp.csic.es (L.M.-N.); cristina.alvarez@ictp.csic.es (C.Á.); lozano@ictp.csic.es (Á.E.L.)
- ² Surfaces and Porous Materials (SMAP, UA-UVA_CSIC), Associated Research Unit to CSIC, University of Valladolid, Paseo Belén 7, E-47011 Valladolid, Spain
- ³ Department of Chemical and Biomolecular Engineering, Universidad de Cantabria, E-39005 Santander, Spain; jorge.moranchel@alumnos.unican.es
- ⁴ IU CINQUIMA/Química Inorgánica, Facultad de Ciencias, Universidad de Valladolid, E-47071 Valladolid, Spain
- * Correspondence: casadoc@unican.es

Abstract: Mixed matrix membranes (MMMs) provide the opportunity to test new porous materials in challenging applications. A series of low-cost porous organic polymer (POPs) networks, possessing tunable porosity and high CO₂ uptake, has been obtained by aromatic electrophilic substitution reactions of biphenyl, 9,10-dihydro-9,10-dimethyl-9,10-ethanoanthracene (DMDHA), triptycene and 1,3,5-triphenylbenzene (135TPB) with dimethoxymethane (DMM). These materials have been characterized by FTIR, ¹³C NMR, WAXD, TGA, SEM, and CO₂ uptake. Finally, different loadings of these POPs have been introduced into Matrimid, Pebax, and chitosan:polyvinyl alcohol blends as polymeric matrices to prepare MMMs. The CO₂/CH₄ separation performance of these MMMs has been evaluated by single and mixed gas permeation experiments at 4 bar and room temperature. The effect of the porosity of the porous fillers on the membrane separation behavior and the compatibility between them and the different polymer matrices on membrane design and fabrication has been studied by Maxwell model equations as a function of the gas permeability of the pure polymers, porosity, and loading of the fillers in the MMMs. Although the gas transport properties showed an increasing deviation from ideal Maxwell equation prediction with increasing porosity of the POP fillers and increasing hydrophilicity of the polymer matrices, the behavior of biopolymer-based CS:PVA MMMs approached that of Pebax-based MMMs, giving scope to not only new filler materials but also sustainable polymer choices to find a place in membrane technology.

Keywords: gas separation; Matrimid; Pebax; biopolymers; mixed matrix membranes (MMMs); porous organic polymers (POPs); CO₂/CH₄ separation; Maxwell phenomenological equations



Citation: Matesanz-Niño, L.; Moranchel-Pérez, J.; Álvarez, C.; Lozano, Á.E.; Casado-Coterillo, C. Mixed Matrix Membranes Using Porous Organic Polymers (POPs)—Influence of Textural Properties on CO₂/CH₄ Separation. *Polymers* **2023**, *15*, 4135. <https://doi.org/10.3390/polym15204135>

Academic Editor: Francesco Galiano

Received: 16 September 2023

Revised: 15 October 2023

Accepted: 15 October 2023

Published: 18 October 2023



Copyright: © 2023 by the authors. Licensee MDPI, Basel, Switzerland. This article is an open access article distributed under the terms and conditions of the Creative Commons Attribution (CC BY) license (<https://creativecommons.org/licenses/by/4.0/>).

1. Introduction

The present concern of the current climate emergency is stirring worldwide interest in the development of materials and technologies for the decarbonization of industry and society by CO₂ capture, clean energy production, and biogas upgrading. Biogas upgrading offers the possibility to recover both methane and carbon dioxide for ulterior utilization [1]. Membrane technology for the simultaneous recovery of CO₂ and CH₄ fluxes from different sources will play a key role in the development of industrial materials with higher efficiency than current ones [2–4]. Commercially available membranes have performed well in CO₂/CH₄ separation on the pilot scale, as Sepuran[®] [5], Polyactive[™] [6], and Polaris[®] [7]. The well-known trade-off between permeability and selectivity in polymeric membranes has been a major drawback for the larger deployment of membrane technology in CO₂

separation applications, together with the issue of uncertainty regarding stability in real industrial feed gas streams [8–10], leading to the development of new materials to face the challenges of existing ones. Most of the studied materials in CO₂/CH₄ separation are based on polyimides [11] and block co-polymers [12]. Most recently, the focus has been turned to biopolymers and materials from renewable sources [13,14] such as chitosan [15].

Attempts have been made to overcome these issues by well-designed mixed matrix membrane material (MMMs), involving the loading of polymer matrices with small amounts of advanced fillers to obtain synergistic properties between the two components [16]. Interfacial control in mixed matrix membranes has always been an issue to be solved. This point has been addressed by the outcome of porous organic materials, or COMs, selective for the gases of interest, as fillers into polymeric membranes, because their organic nature allows the expectation of higher selectivity than zeolite or metal oxide fillers. Porous covalent–organic materials (COMs) have high surface areas and diverse pore dimensions, topologies, and chemical functionalities, for which they are attracting interest in a range of scientific fields, from gas storage to energy applications [17]. Porous polymer networks (PPNs) offer high free volume and CO₂ uptake [18]. There are several good perspectives, reviews, and research articles on different kinds of such organic porous fillers, from metal organic frameworks [19] and covalent organic frameworks [20] to porous organic cages (POCs) [21], amorphous scrambled derivatives (ASPOCs) [22], porous organic frameworks (POFs) blended with polysulfone [23], supramolecular organic frameworks combined with Matrimid [24], and hydrogen-bonded porous polymers blended with Pebax 1657MH [25]. Note that most of the studies are focused on the characterization of the POP particles and their effect on improving the permselectivity of conventionally not highly permeable or selective well-known polymers. Most of these studies, as reflected in Table 1, are dealing with the synthesis and characterization of the materials. The only hint about the gas separation performance is given by time-lag single gas permeation measurements in a constant volume setup. MMMs were prepared on commercial polymers with low permeability and/or selectivity such as Matrimid and Pebax, to evaluate the influence of the loading of the new porous fillers. As far as we know, only Gao et al. [23] used 50:50 (*v/v*%) binary gas mixtures of CO₂/CH₄ and CO₂/N₂ to characterize the separation performance. More recently, Wang et al. studied the effect of humidity in mixed gas separation performance, at a concentration of 30:70 (*v/v*%) for the case of CO₂/CH₄ separation [25].

The understanding of this interaction has been modeled with several phenomenological model approaches based on the Maxwell equation, enabling the correlation between the permeability of novel membrane materials from the components of the blend or mixture. Recent reviews have shed light on research efforts that account for non-idealities in the behavior of Maxwell's equation for different MMMs, through attempts to quantify chain rigidification and interfacial distances between the dispersed filler and the polymer continuous phases [26], as a function of the volume fraction and dispersion of the porous filler and the permeability of the gas components through the dispersed and continuous phases. The understanding of the CO₂ separation performance of MMMs filled with porous organic networks has also been envisaged by the Maxwell equation, for MWNTs in Pebax [27], knitting aryl polymers, KAPs, in polycarbonate [28], and imine/imide porous organic cages in Matrimid [21]. Recently, a hydrophobic amorphous porous organic polymer (POP-2) containing triaryl amines linked by 1,4-diethynylphenyl bridges was compared as filler to Matrimid with metal–organic frameworks such as ZIF-8 and Cu-BTC, regarding the CO₂ permeability in the presence of H₂S impurities [29]. However, the lack of sufficient experimental data on the permeability of CO₂ and CH₄ through the porous organic polymer dispersed phases in MMMs, makes necessary the definition of parameters to estimate the membrane design requirements for a certain CO₂/CH₄ separation. Minelli et al. [30] use the ratio α , i.e., the permeability ratio between the dispersed and continuous phases to be able to compare the Maxwell model equation considering different morphologies and interaction between the phases: (i) parallel orientation of the particles to the direction of the flux, (ii) normal or in series, (iii) Maxwell model for spherical particles, and (iv) Wiener's

equation introducing the different shape factor or the dispersed phase within the continuous matrix. These phenomenological model approaches fail to describe the large differences observed in MMMs when highly porous fillers, such as carbon molecular sieves (CMS) and ad-hoc modification consisting of applying these model equations twice to account for the interface between the particle and the polymer matrices, were proposed to predict the non-ideal performance of polyimide-filled MMMs [31]. The development of complex polymer matrices by co-polymerization [32,33] and the recent attention of researchers on the potential of bio-based polymers and fillers in membrane separation makes room for unexplored non-idealities worth understanding [13,34,35].

Table 1. Mixed matrix membranes reported from porous organic polymer networks for CO₂/CH₄ separation.

| Porous Organic Filler | Polymer Matrix | Filler Loading (wt.%) | P(CO ₂) (Barrer) | CO ₂ /CH ₄ Selectivity | Other Characterization |
|----------------------------|-----------------------------|-----------------------|------------------------------|----------------------------------------------|-----------------------------------------------------------------------------------------------------------------------------------------------------------------------------------------------|
| Pillar [5] arene, SOF [24] | Matrimid 5218 TM | 0 | 73 ± 2 | 27 ± 5 | Single gas permeation, 20 °C, 1 atm PXRD, SEM |
| | | 10 | 63 ± 4 | 31 ± 7 | |
| | | 50 | 75 ± 4 | 25 ± 4 | |
| POP2 [29] | Matrimid 5218 | 20 | 26.9 ± 1.0 | 35.86 | Pure gas permeability in the absence and presence of H ₂ S in CH ₄ and/or N ₂ |
| POCs [21] | Matrimid 9725 | 0 | 10.8 | 31.1 | Single gas permeation ¹ H NMR, SEM, PXRD, SXRD, ATR-FTIR, TGA, gas sorption at 273 K and 25 °C, BET Mixed gas CO ₂ :CH ₄ (1:1) Permeation, 298 K |
| | | 20 | 16.7 | 41.7 | |
| | PEEK-WC | 0 | 6.04 | 23.9 | |
| | | 20 | 6.15 | 25.7 | |
| SNW-1 [36] | Polysulfone (PSf) | 0 | 8.00 | 17.5 | ¹³ C CP/MAS NMR, ¹⁵ N CP/MS NMR, TGA, mechanical properties, SEM, FTIR, BET |
| | | 12 | 22.4 | 34 | |
| HOF-21 [25] | Pebax MH 1657 | 0 | 240 | 8 | FTIR, ¹³ C NMR, SEM-EDX, TGA, PXRD, DFT |
| | | 3 | 780 | 40 | |

In a previous work, a POP material derived from 4,5-diazafluoren-9-one (DAFO) and 1,3,5-triphenylbenzene (135TPB) containing bipyridine functionality was characterized as filler in Matrimid mixed matrix membranes regarding single gas permeability of CO₂, CH₄ and N₂, and olefin/paraffin separation [37]. In this work, five different hyper-crosslinked porous organic polymers (POPs) synthesized at the Institute of Polymer Science and Technology (ICTP-CSIC) were added as dispersed fillers to three different polymers in CO₂ separation as continuous matrices, in order to evaluate the potential of novel materials in CO₂ separations. The effect of porosity and CO₂ uptake properties of the POPs on the permeability and selectivity of the resulting membranes was assessed. The polymers chosen for the continuous matrix were Pebax (60%/40%) and a 50:50 *v/v*% blend of biopolymer chitosan (CS) and biodegradable low-cost polymer polyvinyl alcohol (PVA), in quest of the circularity of membrane preparation [13]. The performance of the membranes was analyzed by mixed CO₂/CH₄ gas separation and compared with previous work where a POP filler similarly containing bipyridine functionality was used as filler in Matrimid MMMs, regarding the single gas permeability of CO₂, CH₄ and N₂, and olefin/paraffin separation [37]. The performance of the gas separation was analyzed in terms of phenomenological model equations to evaluate the deviations from previously reported MMM behavior [38].

2. Materials and Methods

2.1. Materials

Matrimid 5218 (made from 3,3',4,4'-benzophenone tetracarboxylic dianhydride and diaminophenylindane) was supplied by Hunstman (Merrimack, NH, USA). Pebax[®] 1657 MH was supplied by Arkema (Colombes, France). Chitosan (CS) was purchased from Sigma Aldrich (deacetylated degree 75% and molecular weight 310,000 to 375,000). Polyvinyl alcohol (PVA, 99+% hydrolyzed, with a molecular weight 85,000 to 124,000 g/mol) was also purchased by Sigma Aldrich (Madrid, Spain).

2.2. Synthesis Procedures

The POPs were synthesized by the reaction of aromatic trifunctional symmetric monomers (tritycene and 1,3,5-triphenylbenzene, 135-TPB) separately, together, or copolymerized with bifunctional aromatic monomers, as biphenyl and 9,10-dihydro-9,10-dimethyl-9,10-ethanoanthracene, DMDHA, using dimethoxymethane (DMM) as a linker promoter in the presence of a Lewis acid catalyst (FeCl₃). Table 2 collects the composition of the POPs prepared for this work and the initial molar proportion of monomers and starting reactants from the aromatic molecules whose chemical formula is represented in Figure 1. The solvent dichloroethane was added in 15–30 times volume to the mmol of DMM (v/mol). The reaction temperature was set to 60 °C for 72 h.

Table 2. The molar composition of monomers and reactants used in the syntheses of the POP fillers in this work.

| POP | Triptycene | 135-TPB ¹ | Biphenyl | DMDHA ² | DMM ³ | FeCl ₃ |
|------|------------|----------------------|----------|--------------------|------------------|-------------------|
| POP1 | 1 | - | - | - | 3 | 3 |
| POP3 | 1 | - | - | 0.67 | 4.33 | 4.33 |
| POP4 | 1 | - | 0.67 | - | 4.33 | 4.33 |
| POP6 | - | 1 | - | - | 3 | 3 |
| POP9 | - | 1 | - | 0.67 | 4.33 | 4.33 |

¹ 135-TPB = 1,3,5-triphenylbenzen; ² DMDHA = 9,10-dihydro-9,10-dimethyl-9,10-ethanoanthracene; ³ DMM = Dimethoxymethane.

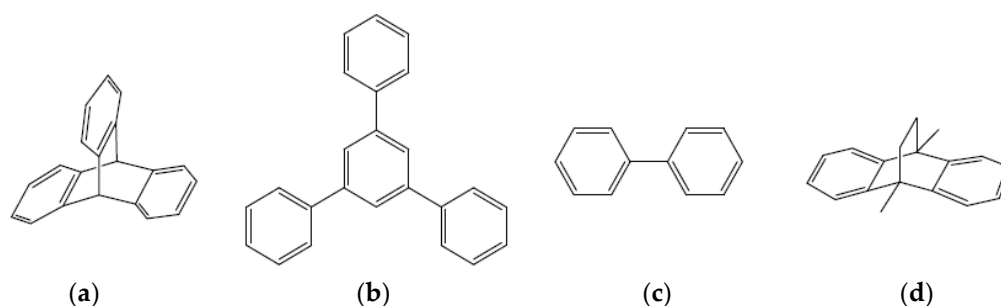


Figure 1. Bifunctional and trifunctional aromatic molecule constituents of the POP structure: (a) triptycene, (b) 135-TPB, (c) biphenyl, (d) DMDHA.

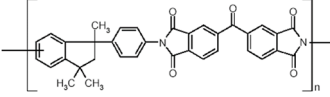
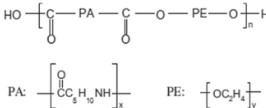
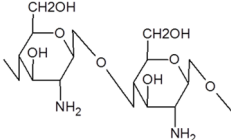
Synthesis of Polymer Membranes

Membranes were prepared by adding different filler loadings from 0 to 10 wt.% to the total polymer content of the different POPs in different polymers whose main physical properties are collected in Table 3.

Matrimid membranes were prepared as reported elsewhere [37], by dissolving 450 mg Matrimid in 10 mL chloroform (Scharlau) under magnetic stirring for 24 h at room temperature. The solution was then poured on a leveled glass plate kept at room temperature, limited by a glass ring to obtain a homogeneously thick film. To avoid fast evaporation of the solvent, the ring was slightly covered with a glass funnel. The film resulting after solvent evaporation was removed from the glass plate and treated in a vacuum oven (Heraeus

Vacuum) at 60 °C (90 min), 120 °C (120 min), 150 °C (60 min), and 220 °C (60 min) and cooled down slowly in the oven. The average membrane thickness was $50 \pm 3 \mu\text{m}$.

Table 3. Properties of the polymers used as continuous matrices for MMM preparation.

| Property | Matrimid 5218 | Pebax MH 1657 | Chitosan |
|----------------------------------|-----------------------------------------------------------------------------------|------------------------------------------------------------------------------------|-------------------------------------------------------------------------------------|
| Chemical structure |  |  |  |
| T _g (°C) | 317 [39]; 308 [40] | −53 | 203 [41] |
| Density (g cm ^{−3}) | 1.225 [42] | 1.14 | 0.942 [43] |
| Melting point (°C) | >300 [40] | 204 ¹ | 270 [44] |
| Estimated fractional free volume | 0.21 [45] | 0.143 [46] | 0.228 [47] |

¹ Data provided by the supplier.

Pebax membranes were prepared by dissolving 3 wt.% Pebax in a 70:30 *v/v*% ethanol/water mixture at 90 °C for 6 h, then removing the bubbles if needed by using an ultrasound bath for 10 min, and casting on hydrophobized glass Petri dishes of 4.5 cm diameter. The solvent was evaporated in a fume hood for 24–48 h, slightly covered at room temperature, then dried in a vacuum at 40 °C to a constant weight, and removed from the glass plate.

CS:PVA membranes were prepared as reported elsewhere [48], from equivalent volumetric blends of CS 1 wt.% solution in 2 wt.% aqueous acetic acid solution and PVA 4 wt.% aqueous solutions prepared independently by stirring at room temperature and under reflux at 80 °C for 24 h before blending. The membranes were likewise cast in Petri dishes and the solvent evaporated for 2–3 days at room temperature in a fume hood and neutralized by immersion in NaOH 1 M solutions for 1 h, then rinsed with DI water to be removed from the glass [49,50].

Mixed matrix membranes were prepared by adding polymer solutions to the suspension of the POP material in 2 mL of the corresponding solvent. In the case of the Matrimid-based MMM, it was necessary to sonicate the suspension for 20 min before casting, to avoid agglomerates [37]. In the case of Pebax-based MMMs, the POPs were previously treated with air-based low-pressure plasma (Piezo brush[®] PZ3, Reylon plasma, Regensburg, Germany) for 30 s to hydrophilize the surface [51] and ease the compatibility with the Pebax matrix. In the case of Pebax-based MMMs, the POPs were previously treated with air-based low-pressure plasma (Piezo brush[®] PZ3, Reylon plasma) for 30 s to hydrophilize the surface [51] and ease the compatibility with the Pebax matrix. This was not necessary for the CS:PVA membranes, which was attributed to the high hydrophilicity of the biopolymers, which compensated for the differences between the dispersed and continuous phases in the membrane matrix. The particle loadings of POP in the MMMs were calculated as

$$\varnothing_d = \frac{\text{weight of particle}}{(\text{weight of particle} + \text{weight of polymer})} \times 100 \quad (1)$$

2.3. Characterization

ATR–FTIR experiments were conducted on the POP and membrane samples using a Spectrum 65 Spectrophotometer (Perkin Elmer, Waltham, MA, USA) at a 4 cm^{−1} resolution and 8 scans per measurement, in the range of wave numbers of 4000–400 cm^{−1}.

¹³C NMR of the POPs were registered in a solid-state Avance TM 400 WB (Bruker, Mannheim, Germany), equipped with a superconductor wide magnet (89 mm) operating at 9.4T, using cross-polarization (CP) and magic angle spinning (MAS). The spectra were

registered at a frequency of 100.6 MHz and contact pulses of 1 ms, with a delay time of 3 s, and a spinning speed of 11 kHz.

The WAXD diffractograms of POPs were registered at room temperature in a Bruker D8 Advance diffractometer, equipped with a Cu X-ray source (wavelength $\lambda = 1.54 \text{ \AA}$, a Göbel mirror, and a Vantec detector, at a step of 0.024° and a rate of 0.5 s/step , in the interval of 2θ from 3 to 60° .

SEM images were obtained using a scanning electronic microscope with field emission filament QUANTA 200 FEG ESEM, Hillsboro, OR, USA. The membrane film samples were prepared by cryogenic fracture after immersion in liquid nitrogen, and they were Au-metallized.

The skeletal density of POPs was measured in a He pycnometer (AccuPyc, Micromeritics). The density of the polymer and mixed matrix membranes was estimated from the weights and thicknesses of the circular pieces of membranes before and after gas separation experiments [47].

Adsorption/desorption isotherms of the POPs were measured in a N_2 volumetric analyzer (ASAP2020, Micromeritics) at 77 K of the previously degassed samples at 200°C for 16 h . The surface area was calculated from the adsorption isotherms by the Brunauer–Emmett–Teller (BET) method, and the pore volume was obtained at a relative pressure of around $p/p_0 = 0.98$. The microporosity of samples was estimated by the t-plot method. CO_2 uptake in the POP fillers was conducted in a Cahn D200 microbalance at 25°C [37].

Thermogravimetric analyses (TGA) were realized in a TA-Q500 (TA instruments, New Castle, DE, USA) for the POPs at a heating rate of 10°C in the interval of $30\text{--}850^\circ \text{C}$ under N_2 (50 mL/min) whereas $1\text{--}5 \text{ mg}$ membrane samples of the films were measured at a TGA–DTA Shimadzu (Kyoto, Japan) in the range of $25\text{--}600^\circ \text{C}$ at a heating rate of 20°C/min , also under N_2 flow of 50 mL/min [52].

The thickness of the MMMs was determined by a Mitutoyo IP-65 with a precision of 0.001 mm , at 5 different spots on the membrane surface area after synthesis. The standard deviation of these measurements was below 0.003 cm for all the membranes under study.

2.4. Gas Transport and Separation

Single gas permeability values of He, H_2 , CO_2 , N_2 , and CH_4 gases across the neat polymer and MMMs were determined at 30°C and a feed pressure of 3 bars, in a constant volume/variable pressure system at the ICTP–CSIC (Madrid, Spain). Before each measurement, the membrane was kept in a high vacuum overnight to remove humidity and solvent traces. The absence of pinholes was checked by He permeation, at pressures between 1 and 5 bars. The membrane was then subjected to a gas pressure of 3 bars, and the rise of permeate pressure (gas through the membrane) was monitored as a function of time until a steady stationary state was attained, where the relationship between permeate pressure and time was linear.

The permeability of the membrane, P , in steady-state conditions, was calculated by

$$P = \frac{273.15}{76} \frac{V \cdot l}{A \cdot T \cdot p_0} \frac{dp(t)}{dt} \quad (2)$$

where V , cm^3 (STP), is the volume of the low-pressure compartment, l , cm, the membrane thickness, A , cm^2 , the effective surface area of the membrane, T , K, the working temperature, p_0 , bar, the feed gas pressure, $dp(t)/dt$, mbar/s, the slope of the straight line. The relative error of this calculation procedure was below 10%.

The extrapolation of the straight line of the time-lag graph allows for determining the time lag, θ , necessary to reach the steady state, from which the value of the diffusivity coefficient can be determined as

$$D = \frac{l^2}{6\theta} \quad (3)$$

The solubility coefficient, S , is thus calculated indirectly, by the solution–diffusion model relationship between permeability and diffusivity coefficients [53]

$$S = \frac{P}{D} \quad (4)$$

The ideal selectivity of a membrane for a gas pair separation A/B is usually determined by the ratio between the fast and slow permeabilities of the gases A and B,

$$\alpha_{A/B} = \frac{P_A}{P_B} \quad (5)$$

Mixed gas separation of CO₂:CH₄ 50:50 v/v% mixtures was performed in a homemade bench-scale separation plant built at the UC [54]. The feed pressure was set at 4 bars and the composition of the feed was set by Kofloc mass flow controllers. The permeate composition was measured by an IR gas analyzer (BIOGAS 5000, Fonotest, Madrid, Spain), and the permeate flow rate by a bubble flowmeter.

3. Results

3.1. Characterization of Materials and Membranes

3.1.1. Physico-Chemical and Morphological Characterization

The POPs synthesized in this work are hyper-crosslinked materials, and therefore insoluble in organic solvents, hindering their characterization. They were identified by solid NMR and FTIR spectroscopies, although FTIR could not confirm the chemical structure due to the low intensity of the absorption bands attributed to the extreme rigidity and hardness of the material. Figure 2 shows the CP/MAS ¹³C NMR spectra of some of these materials. In general, all POPs presented wide bands that could be assigned to aromatic carbons in the interval between 110 and 150 PPM, as well as the band associated with the CH₂ bridges around 40 ppm.

The porosity of the POPs was evaluated by their skeletal density and the adsorption/desorption isotherms of N₂ at 77 K. Results are summarized in Table 4. The textural properties of the POPs reveal the large surface BET areas of these materials, even compared with analogous materials, which fall below 900 m²/g. POP1, derived from triptycene-DMM, presented the lowest microporosity, and POP6, from triptycene-DMM-biphenyl, presented the highest.

Table 4. Textural properties of the POP fillers studied in this work.

| Type of POP | Skeletal Density (g/cm ³) | S _{BET} (m ² /g) | V _{TOTAL} (cm ³ /g) | V _{MICRO} (cm ³ /g) * | Reference |
|--------------------------------------------|---------------------------------------|--------------------------------------|-----------------------------------------|-------------------------------------------|-----------|
| POP1 | 1.2624 | 1538 | 1.281 | 0.314 | This work |
| POP3 | 1.2051 | 1596 | 1.394 | 0.293 | This work |
| POP4 | 1.1994 | 1318 | 0.727 | 0.368 | This work |
| POP6 | 1.2014 | 1638 | 0.964 | 0.450 | This work |
| POP9 | 1.2288 | 1525 | 1.606 | 0.325 | This work |
| POP2 | 1.33 | 781 | 0.554 | NA | [55] |
| KAP (2Ph-NO ₂) | 1.618 | 605 | 0.313 | NA | [28] |
| KAP (2Ph-CH ₂ NH ₂) | 1.459 | 617 | 0.282 | NA | [28] |
| SNW-1 | NA | 821 | NA | 0.26 | [36] |
| TRPI (135TRP-DAFO) | 1.113 | 806 | 0.42 | 0.24 | [37] |

NA = Not Available. * Volume determined at p/p₀ = 0.9768.

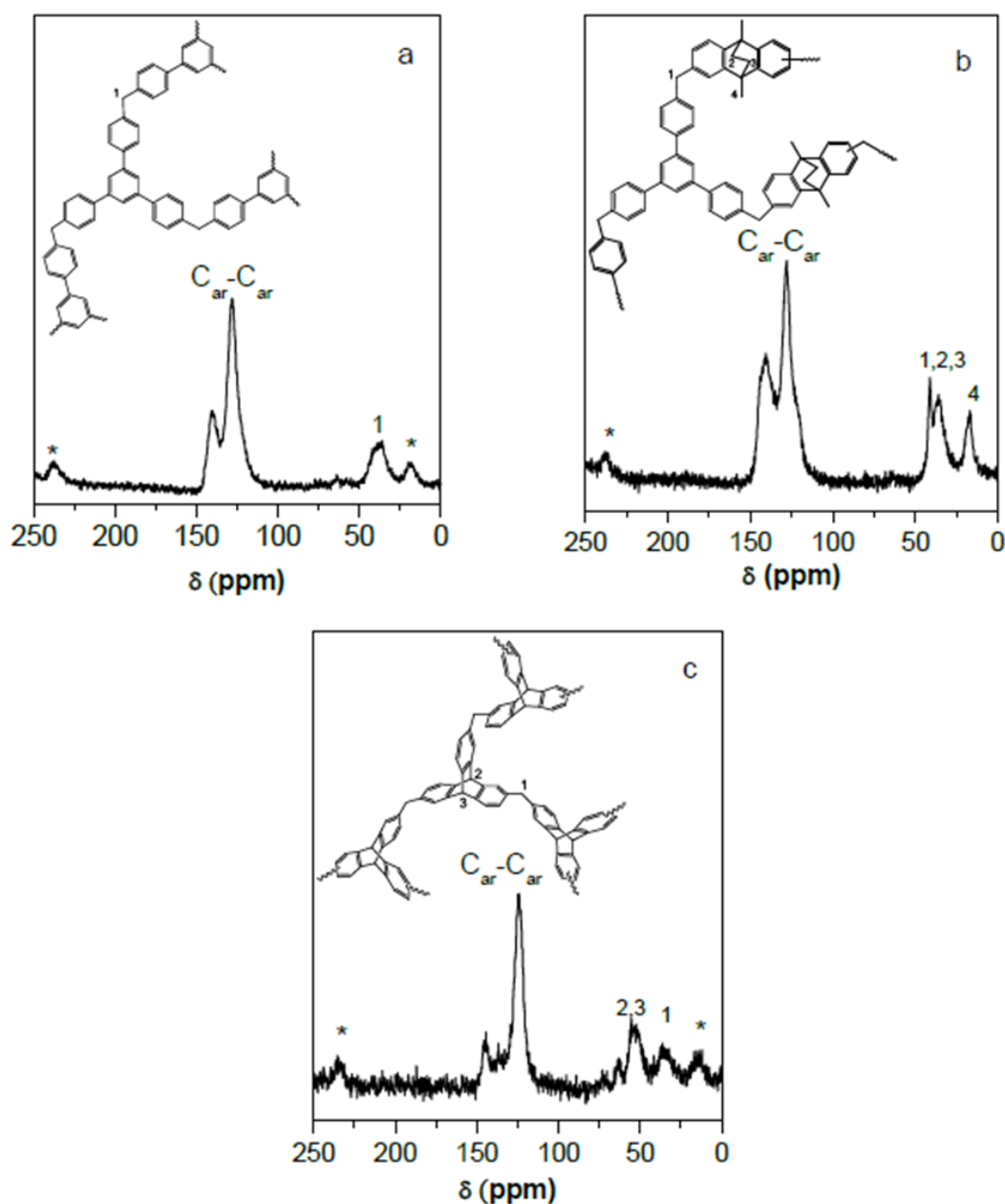


Figure 2. Solid-state CP/MAS ^{13}C NMR spectra of (a) POP6, (b) POP3, and (c) POP1. Asterisks denote spinning side bands.

The porosity of the POPs determines the CO_2 affinity and thereby their use in gas separation. Figure 3 shows the CO_2 uptake measured at 298 K for the POP fillers studied in this work as MMM fillers. The CO_2 uptake ranges from 40 to 70 $\text{mg CO}_2/\text{g}$, in the order $\text{POP4} < \text{POP6} < \text{POP9} < \text{POP3} < \text{POP1}$. Wang et al. reported values of CO_2 uptake up to 45 mg/g and 23 mg/g for the freshly made and NH_2 -functionalized HOF-21 hydrogen organic frameworks [25]. POP2, synthesized from triaryl amines linked by 1,4-diethynyl phenyl, provided a CO_2 uptake of up to 176 $\text{mg CO}_2/\text{g}$, on account of its high porosity, although the micropore volume was not provided [56]. Surprisingly, the POP with the highest CO_2 uptake value was the one with the lowest microporosity and the simplest structure, POP1, and since these values agreed with those reported for SNW-1 by Gao et al. [23], they were attributed to the fact that small pores in the filler material benefited CO_2 affinity, and thus the selective separation of CO_2 (0.33 nm) through those pores.

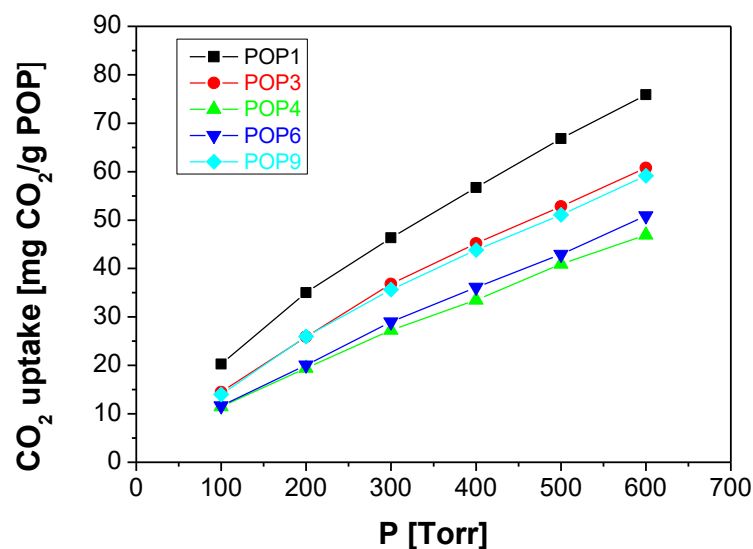


Figure 3. CO₂ uptake at 298 K of the POPs used as fillers in this work.

For these results with the amorphous morphology of the materials, the WAXS spectra of the POPs are represented in Figure 5. All of them show a certain regularity in their chain packing, as reflected by the presence of two well-defined maxima around 2θ values 15° and 45° , respectively. Figure 4 (left) presents the diffractograms of the POPs synthesized from a single triaromatic monomer, as triptycene, or diaromatic, as DMDHA and biphenyl. Comparing all diffractograms, the maximum intensity peak in biphenyl-DMM appears at higher angle values, thus the maximum shifts from 13.6° to 18.5° , which, applying Bragg's law, corresponds to the average preferential distances, d , of 6.49 \AA and 4.79 \AA , respectively. This result can be correlated with the effectiveness of the chain packing observed in POP-4, presumably due to the linear structure of biphenyl, against the non-linear 3D structure of triptycene and DMDHA, inducing the highest regularity in the network [18]. The same behavior is observed in the diffractograms of the right in Figure 5, for POP6 and POP9, derived from triptycene-DMM-DMDHA and triptycene-DMM-biphenyl, respectively.

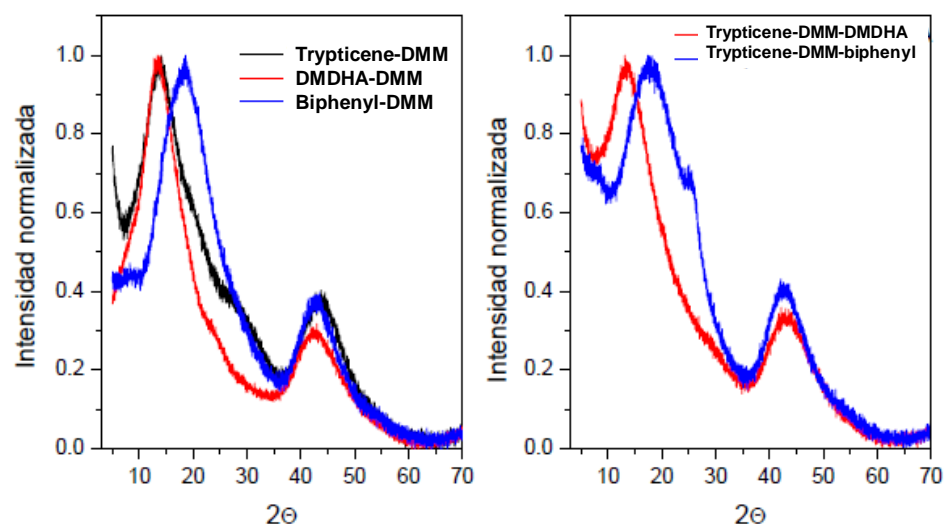


Figure 4. Wide-angle X-ray diffractograms of POP-1, POP-3, and POP-4 (left) and POP-6 and POP-9 (right), normalized against the maximum intensity.

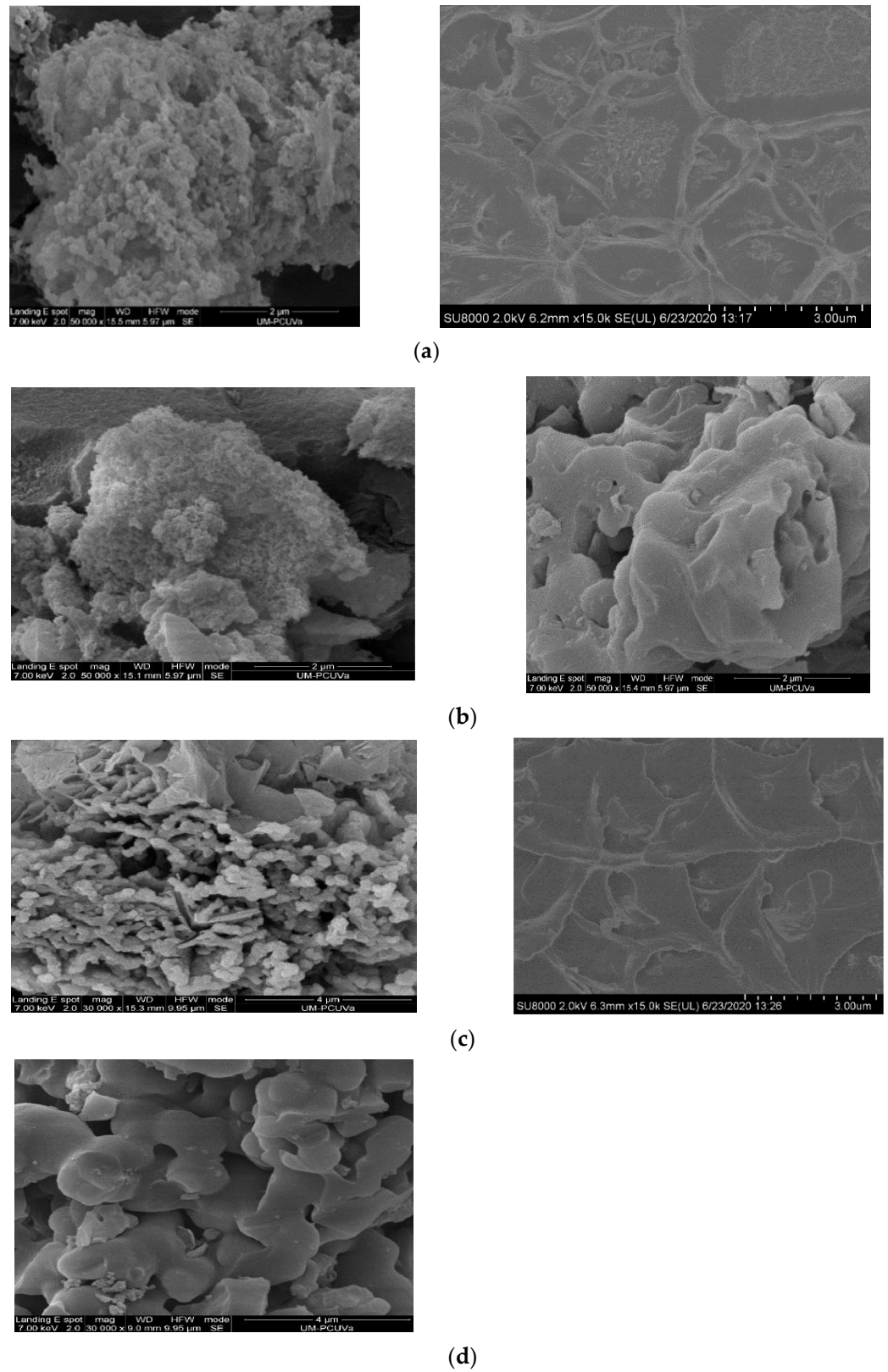


Figure 5. SEM of several POP filler particles are shown in the left, with the cross section of their corresponding MMMs in the right: (a) POP1, (b) POP3, (c) POP4, and (d) POP6, respectively.

More of the amorphous nature of the POPs and their loading into several MMM in Matrimid is discerned in the SEM images in Figure 5. The left column shows the nature of the POP particles, and the differences between POP1 (top-row), POP3, POP4 (third row),

and POP6 (last row), whose porous structure started deteriorating under the electron beam upon observation. The cross sections of POP-1/Matrimid and POP4/Matrimid MMMs are also disclosed on the right column to observe the apparent absence of defects between the particles and the polyimide matrix. Thereby, we can affirm that closely compatible and defect-free membranes have been obtained.

Thermogravimetric analysis curves (TGA) were obtained for both POP fillers and POP-based MMMs under air and N₂ to evaluate the differences in thermal stability of the material in each case. The TGA curves of water-swollen susceptible membranes in N₂ allow analyzing the thermal stability of the membranes as well as quantifying the structural water, which may influence CO₂ transport and separation [52,57]. Figure 6 compares a pristine CS:PVA membrane with CS:PVA membranes filled with 10 wt.% POP as a function of the type of POP. This gives an idea of whether the filler material in the hydrophilic biopolymeric matrix is homogeneously dispersed. There are two major steps, the first one below 100 °C and the second one above 200 °C (the glass transition temperature of pure chitosan is acknowledged to be at 203–206 °C [58]).

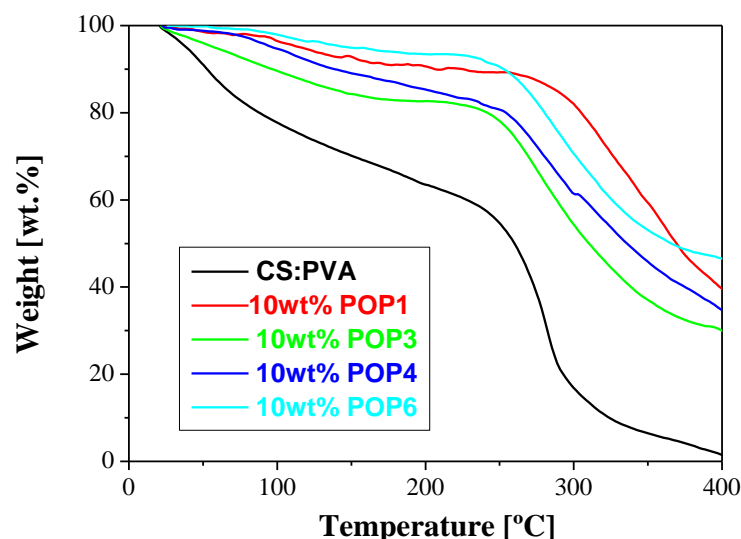


Figure 6. Thermal gravimetric analyses of the POP/CS:PVA MMMs.

The bound water content in hydrophilic membranes was determined according to Franck-Lacaze et al. [52] using Equation (6). This water content (WC) was estimated from the mass samples; m_1 and m_2 , measured at T_1 and T_2 , taken as the minimum observed between the two peaks of the differential spectrum (one for water loss, one for polymer degradation), respectively, which were identified as the main weight losses observed for the CS:PVA membrane in Figure 7.

$$WC(\%) = 100 \times \left(1 - \frac{m_1}{m_2} \right) \quad (6)$$

As an example, Figure 7 represents the TGA analyses under N₂ flow of the POP-6/Pebax membranes at different filler loadings. The largest weight loss due to dehydration occurred below 150 °C for pristine Pebax, and 100 °C for the POP-loaded MMMs, which accounted for the increased hydrophobicity of the POP fillers even after plasma air-treatment. Pyrolysis decomposition occurred between 300 and 450 °C, in agreement with literature [59].

The bound water content can be compared with the water uptake measured by comparing the wet and dry membranes, measured before and after the gas permeation/separation runs, as

$$WU(\%) = \frac{w_{wet} - w_{dry}}{w_{dry}} \times 100, \quad (7)$$

which is also a measure of the swelling of the membranes. The values of total water absorption (WU) and bound water content (WC) were very similar for the CS:PVA membranes, which accounted for the effect of membrane synthesis and POP characteristics on the mechanical robustness of the CS:PVA-based membranes [48]. The swelling of the Pebax-based membranes was so extreme that the WU gave values well over 100%, so the WC values were taken instead in Table 5 for the estimation of the porosity, i.e., void fraction used to estimate the true volume fraction of the dispersed filler within the polymer matrix, as in previous works [50]

$$\varnothing_v = \frac{w_{wet} - w_{dry}}{\rho_w} + \frac{w_{dry}}{\rho_{dry}}, \quad (8)$$

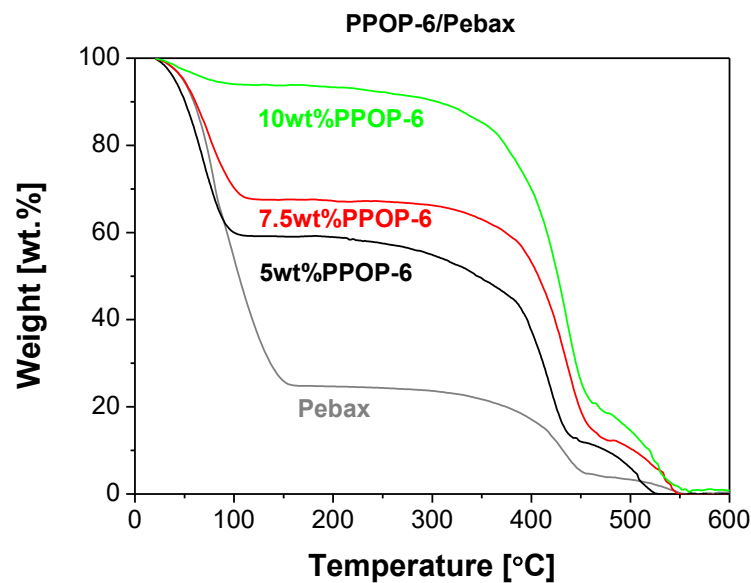


Figure 7. Thermal gravimetric analyses of the POP-6/Pebax MMM as a function of filler loading.

Table 5. Some morphological properties of the MMMs.

| Membrane | Filler wt. Fraction | Thickness (cm) | Density (g/cm ³) | WU (%) | WC (%) | T _d (°C) | Porosity (%) | Volume Fraction, \varnothing_d |
|---------------|---------------------|----------------|------------------------------|--------------|--------|---------------------|--------------|----------------------------------|
| Matrimid [37] | 0 | 0.005 | 1.223 [60] | NA | NA | NA | 16.7 [60] | 0 |
| POP1/Matrimid | 0.20 | 0.005 | 1.232 | | NA | | | 0.195 |
| POP4/Matrimid | 0.20 | 0.005 | | | NA | | | 0.203 |
| Pebax | 0 | 0.01102 | - | (*) | 58 | 290 | - | 0 |
| POP1/Pebax | 0.05 | 0.00772 | 1.124 | (*) | 34 | 172 | 27 | 0.033 |
| POP3/Pebax | 0.05 | 0.00785 | 1.225 | (*) | 59 | 226 | 42 | 0.028 |
| POP4/Pebax | 0.05 | 0.00818 | 1.289 | (*) | 60 | 222 | 44 | 0.027 |
| POP6/Pebax | 0.16 | 0.0189 | 1.009 | 50 | 53.7 | 377 | 40 | 0.091 |
| | 0.32 | 0.0250 | 1.240 | 64 | | 219 | 34 | 0.204 |
| POP9/Pebax | 0.10 | 0.0934 | 1.240 | 64 | 50.8 | 219 | 40 | 0.052 |
| CS:PVA | 0 | 0.016 | 1.749 | 39.80 ± 1.26 | | 131 | 41 | 0 |
| POP1/CS:PVA | 0.05 | 0.0147 | 1.349 | 47.88 | 33 | 171 | 39 | 0.041 |
| | 0.10 | 0.0098 | 1.782 | | 32 | 226 | 48 | 0.070 |
| POP3/CS:PVA | 0.05 | 0.0097 | 2.147 | 37.2 | 40 | 171 | 44 | 0.039 |
| | 0.10 | 0.0136 | 1.305 | | 23 | 172 | 18 | 0.111 |
| POP4/CS:PVA | 0.10 | 0.01185 | 1.389 | 18 | 23 | 172 | 20 | 0.111 |
| POP6/CS:PVA | 0.10 | 0.0133 | 0.850 | 14.5 | 17 | 242 | 11 | 0.124 |

(*) Values over 100% have been removed.

The disparities between the true volume fraction and the nominal mass weight fraction of the filler in the membrane are due to the differences between measured density and the theoretical density values of the MMMs using the additive approach from the densities of their components. These differences have been justified by the presence of non-idealities in the interface between the porous fillers and the polymer chains, because of the partial occupation of the pores by the latter [16,50,61]. Rodriguez-Jardón et al. also observed that the calculated densities were slightly lower than the experimental ones on knitted aryl porous polymer-filled polycarbonate MMMs [28]. The higher densities obtained in the balance weighing of the samples confirmed that the pores of the fillers in the MMMs may be partially occupied by the polymer chains.

3.1.2. Gas Separation and Separation Characterization

The gas separation performance was focused on the separation of CO₂/CH₄ mixtures. The average data of reproducible runs are collected in Table 6, as a function of polymer type, filler type, and membrane thickness. Gas permeation measurement type is indicated since Matrimid membranes were analyzed at ICTP regarding single gas permeation of CO₂ and CH₄, in comparison with previous work on other POP-filled Matrimid membranes [37]. POP1 decreased the CO₂/CH₄ ideal selectivity of pure Matrimid membranes while increasing the CO₂ permeability. The more complex porous network of POP4 was able to maintain the Matrimid CO₂/CH₄ selectivity while increasing the CO₂ permeability almost as much, which accounts for the compatibility observed earlier by SEM.

Table 6. CO₂ permeability and CO₂/CH₄ selectivities and separation factors of the POP-based MMMs studied in this work. Only selective membrane materials are included.

| Polymer Matrix | POP, Filler Loading | Thickness (cm) | P(CO ₂) (Barrer) ^(a) | P(CH ₄) (Barrer) ^(a) | α (CO ₂ /CH ₄) | S.F. (CO ₂ /CH ₄) |
|-------------------------|---------------------|----------------|---------------------------------------------|---------------------------------------------|----------------------------------------------|------------------------------------------|
| Matrimid ^(b) | 0 | 0.005 | 7.84 | 0.186 | 42 | - |
| | POP1, 20 wt.% | 0.005 | 20.68 | 0.632 | 37 | - |
| | POP4, 20 wt.% | 0.005 | 17.0 | 0.400 | 42 | - |
| Pebax ^(c) | 0 | 0.011 | 67.95 ± 13.51 | 4.132 | 16.44 ± 0.31 | 11.78 |
| | POP1, 5 wt.% | 0.077 | 176.95 ± 5.17 | 38.73 | 4.57 ± 0.32 | 3.98 |
| | POP3, 5 wt.% | 0.0078 | 67.95 ± 13.50 | 6.79 | 10.01 ± 3.25 | - |
| | POP4, 5 wt.% | 0.0082 | 180.68 ± 90.54 | 13.50 | 13.38 ± 3.64 | 12.0 |
| | POP6, 16 wt.% | 0.0189 | 1098 | 107.82 | 10.18 | 7.88 |
| | POP6, 32 wt.% | 0.0255 | 428 ± 15.5 | 106.20 | 4.034 ± 0.02 | 3.21 ± 0.04 |
| | POP9, 8.3 wt.% | 0.00632 | 1050 | 1282 | 0.82 | 0.85 |
| CS:PVA ^(c) | 0 | 0.01605 | 51.99 | 1.55 | 33.64 | 31.19 |
| | POP1, 5 wt.% | 0.0147 | 66.15 | 2.06 | 32.14 | 31.43 |
| | POP3, 5 wt.% | 0.0097 | 109.80 | 1.65 | 66.59 | 27.50 |
| | POP3, 10 wt.% | 0.0136 | 36.86 | 2.73 | 13.50 | 13.00 |
| | POP4, 10 wt.% | 0.0118 | 62.81 | 1.19 | 53.00 | 62.5 |
| | POP6, 10 wt.% | 0.0133 | 453.80 | 20.75 | 21.80 | 17.30 |

^(a) 1 Barrer = 10⁻¹⁰ cm³ (STP) cm cm⁻² s⁻¹ cmHg⁻¹; ^(b) time-lag experiments performed at the University of Valladolid, as in [37]; ^(c) mixed gas separation experiments with a 50:50 (v/v%) CO₂:CH₄ feed mixture at the University of Cantabria, as in [54].

The performance of Pebax- and CS:PVA-based membranes was measured using a 50:50 (v/v%) CO₂:CH₄ mixed gas feed at the bench scale separation plant built at UC [54]. The results are summarized in Table 6. In general, it can be observed that the CO₂ permeability of Pebax membranes was also influenced by the type of POP added to the Pebax matrix, in the order POP6 > POP1 > POP4 > POP3, while the CO₂/CH₄ selectivity was maintained in the same order of magnitude (between 10 and 16) except for the POP1/Pebax MMM, which decreased with increasing filler loading, as observed for POP-6. The 20 wt.% loading of the Matrimid matrix did not increase the selective performance of this polyimide. As for the new biopolymer-based CS:PVA-based MMMs, the CO₂ permeability also increased

in the order POP6 > POP4 > POP3 > POP1, which can be correlated with the hydrophilic nature of the CS:PVA matrix governing the interaction with the porous organic particles, since selectivity decreased in reverse order. Thus, the 10 wt.% POP3/CS:PVA membranes showed lower selectivity than the 5 wt.% POP3/CS:PVA membrane.

The selectivity performance of the POP-filled MMMs for CO₂/CH₄ separation is illustrated together with the Robeson plots in Figure 8. The Robeson plots indicated in the graph are those reported by Robeson himself in 1991 [62] for the first polymer films with gas permeation data and the updated ones in 2008 with new polymer advancements and gas pair mixtures [63]. The line named “Robeson (2019)” is the one updated by Comesaña-Gandara et al. to consider specifically the separation of CO₂ from other gases typical in industrial effluent [10]. We can observe that POP1- and POP4-based CS:PVA MMMs surpass the state-of-the-art in polymer membranes for the separation of CO₂/CH₄ gas pairs, while the Pebax membranes prepared in this work do not. This result may be attributed to the difficulty of making Pebax membranes with these types of filler that need to be functionalized further for compatibility. Wang et al. [25] functionalized their HOF-21 with NH₂ groups to obtain a defect-free membrane enabling the evaluation of the influence of the hydrogen organic framework in the Pebax matrix.

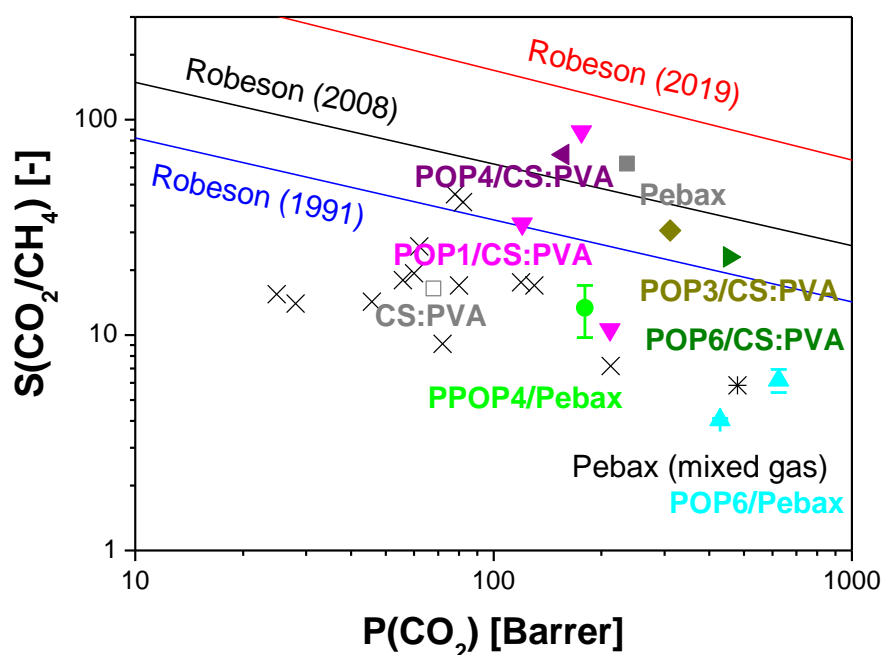


Figure 8. Robeson upper bound for CO₂/CH₄ separation. The cross points correspond to values of single gas permeation through pristine Pebax membranes in the literature. The double cross points are the values reported for the separation of CO₂/N₂/CH₄ ternary mixture by Montes de Luna et al. [64]. The color points are the values of mixed gas separation performance for the POP/Pebax and POP/CS:PVA mixed matrix membranes measured in this work.

The separation factor of the gas mixture presented in Table 6 for CS:PVA-based MMMs was calculated from the concentration of slow and fast gas permeating molecules in the feed and permeate streams respectively. We can observe that the separation factor agreed with the ideal selectivity calculated by Equation (5), which can be assigned to good compatibility between the CS:PVA continuous matrix and the POP fillers. Clearly, the plasma treatment of the POP particles was not enough to improve their compatibility with Pebax, and non-idealities occurred that will be analyzed below.

3.2. Mechanism of Transport through MMMs

An investigation of the overall permeability behavior of new mixed matrix membranes involving a dispersed phase (filler) or a continuous phase (polymer matrix) is essential to

obtain new materials with improved properties. The main modeling parameters are: (1) the single gas permeability coefficients of the component of the feed mixture (assuming they are independent of the concentration of the permeating species in a mixed gas environment), (2) the composition of the MMM, expressed as the true volume fraction of the dispersed filler, and (3) the shape and arrangement of the dispersed particles in the MMM.

The most used phenomenological model to describe MMM transport properties is the Maxwell equation that describes the overall permeability through a composite medium of a highly diluted dispersion of congruent spheres in a continuous phase, where interparticle distances are large enough to ensure that the permeant flow pattern around each particle is not disturbed by the presence of the others. This equation can be written as

$$P_{MMM} = P_c \left[\frac{P_d + 2P_c - 2\varnothing_d(P_d - P_c)}{P_d + 2P_c + \varnothing_d(P_d - P_c)} \right], \quad (9)$$

where P_{MMM} is the effective permeability of the mixed matrix membrane material, P_c is the permeability of the continuous polymer phase, measured experimentally on the pristine polymer membrane, and P_d is the permeability of the dispersed filler phase, respectively. \varnothing_d is the true volume fraction of the dispersed filler (Table 4). Since MMMs are often made from novel filler materials never tested as membranes before, as is the case with POPs, Equation (9) has been rearranged as follows [65]:

$$P_{MMM} = P_c \left[1 + \frac{3\varnothing_d}{(\alpha + 2)(\alpha - 1) - \varnothing_d} \right] \quad (10)$$

where $\alpha = P_d/P_c$ is an adjustable parameter. Rodriguez-Jardón et al. [28] simplified it further for porous organic fillers by defining a new parameter β , accounting for the reduced permeation polarizability observed in polyimide-like polymer matrices, and only depending on gas permeabilities.

$$P_{MMM} = P_c \left[\frac{2(1 - \varnothing_d) + \alpha(1 + 2\varnothing_d)}{(2 + \varnothing_d) + \alpha(1 - \varnothing_d)} \right] = P_c \frac{1 + 2\varnothing_d}{1 - \beta\varnothing_d} \quad (11)$$

where

$$\beta = \frac{\alpha - 1}{\alpha + 2} = \frac{P_d - P_c}{P_d + 2P_c} \quad (12)$$

Figure 9 uses these analyses to evaluate the CO₂ permeability of the POP membranes prepared in this work, with parameter β ranging from -1 to 12.5 . Literature trying to describe the gas transport through MMMs varied this parameter between -0.5 and 1.0 to represent non-permeable and wholly permeable fillers. The value of $\beta = 0$ meant a value for α having equal permeability in both continuous and dispersed phases. As with them, our POPs are porous and thus totally permeable so β should be closer to 1 .

As expected, since the Maxwell model equation assumed the diluted dispersion of spherical particles, the performance of the higher-porosity fillers like POP9- and POP6-based membranes deviated from the description of this model. A first evaluation of the prediction capability of the gas transport properties through a new MMM involved evaluating the limits of the Maxwell equation. The minimum and maximum limits of the Maxwell equation have also been expressed as a function of the membrane composition and the differences in permeability through the continuous and dispersed phases, by considering a series mechanism of transport through the dispersed and continuous phases as

$$P_{MMM} = \frac{P_c P_d}{(1 - \varnothing_d)P_d + \varnothing_d P_c} = P_c \left[1 + \varnothing_d \left(\frac{1}{\alpha} - 1 \right) \right]^{-1} \quad (13)$$

and the maximum value is assumed when both phases contribute in parallel to the flow direction,

$$P_{MMM} = \varnothing_d P_d + (1 - \varnothing_d)P_c = P_c [1 + \varnothing_d(\alpha - 1)] \quad (14)$$

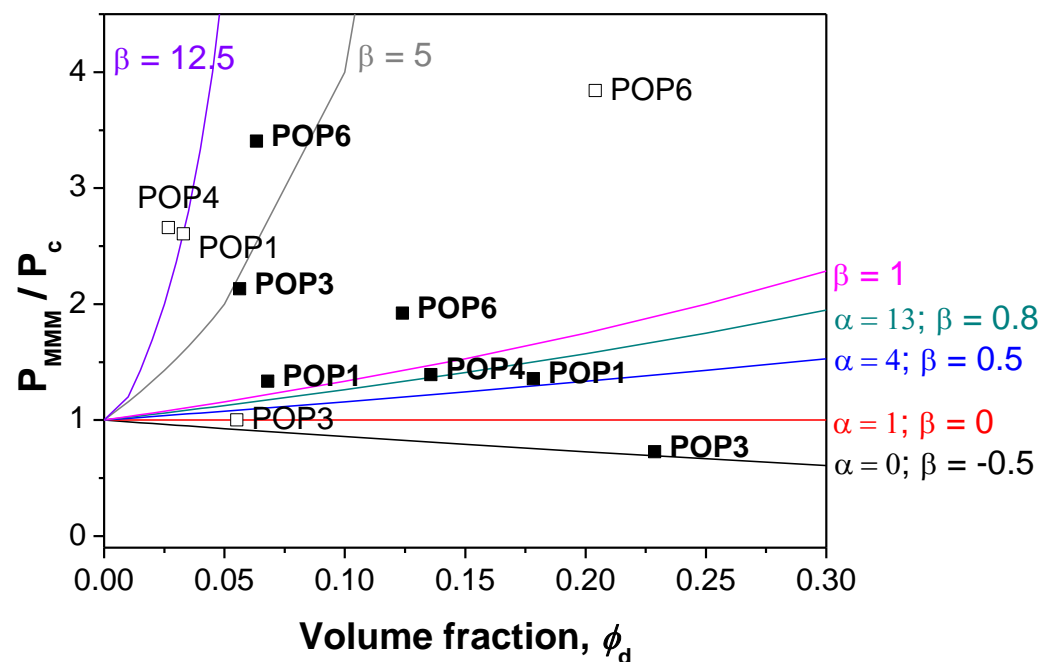


Figure 9. Comparison between the experimental data for CO₂ permeability through POP-filled Pebax and CS:PVA MMMs and the Maxwell model predictions using Equations (10) and (11).

The accuracy between the experimental values (Table 6) and the values predicted with Equations (9), (13) and (14) has been compared in terms of the percentage average absolute error (AARE) and collected in Table 7.

Table 7. Percentage (%) of average absolute relative error (AARE) for the sum of calculated CO₂ and CH₄ permeation prediction for each MMM.

| Continuous Matrix | Dispersed Phase | Parallel | Series | Maxwell |
|-------------------|-----------------|----------|--------|---------|
| Matrimid | POP1 | 13.11 | 15.26 | 11.18 |
| | POP4 | 5.12 | 22.26 | 17.12 |
| Pebax | POP1 | 31.02 | 31.13 | 31.05 |
| | POP3 | 0.48 | 0.74 | 4.40 |
| | POP4 | 31.37 | 31.46 | 31.39 |
| | POP6 | 42.6 | 42.8 | 6.42 |
| | POP9 | - | - | - |
| CS:PVA | POP1 | 10.96 | 10.99 | 10.97 |
| | POP3 | 26.47 | 26.50 | 27.38 |
| | POP4 | 51.09 | 9.43 | 43.55 |
| | POP6 | 44.38 | 44.39 | 44.38 |

The correlation between overall transport properties and the structure of the interface plays an important role in the development of composite membrane material. Four major cases explaining this correlation when porous fillers are used have been a matter of discussion for a long time [16]. Figure 10 collects the data in Table 5 and Figure 8 in terms of these cases:

- Case 1 corresponds to an ideal behavior or perfect contact between the polymer matrix and the filler.
- Cases II and III are characterized by voids at the interface, causing an increase in permeability without large changes in selectivity, in comparison with pure polymer membranes. In Case II, the effective void thickness is of the order of magnitude of the gas penetrant molecules. Most of the Pebax-based MMMs belong to this range.
- Cases IV and V, where a rigidified polymer region is estimated around the filler causing reductions in permeability and a slight increase in the selectivity of the MMMs in

comparison with the pure polymer membrane. Unsurprisingly, the Matrimid MMMs fall into these categories, and are attributed to the rigidified polyimide structure of Matrimid.

We observe that the POP/Pebax MMMs fall within the category of Cases II and III, on account of the high permeability of Pebax and the porosity of the POPs, especially POP6, imparted to the polymer matrix. Matrimid-based membranes, unsurprisingly, fall close to Cases IV and V, on account of the rigid polyimide matrix of Matrimid. The POP/CS:PVA MMMs fall mid-way, which may be attributed to the semi-crystalline nature of biopolymers and the compatibility with organic fillers with high porosity compatible with the biopolymer functional groups, which may expect some penetration of polymer chains with the POP structure and thus the slight decrease in permeability and increase in selectivity observed for the most porous POPs (POP3, POP6). The tunable hydrophilicity of biopolymers can alter the transport mechanism through the polymer matrix from solution diffusion in TMC-crosslinked chitosan [66], to facilitate transport in swollen chitosan membranes [67]. Pebax could also be blended with biopolymers in this way, as Salestan et al. [68] have reported recently using small loadings of alginate and CMC.

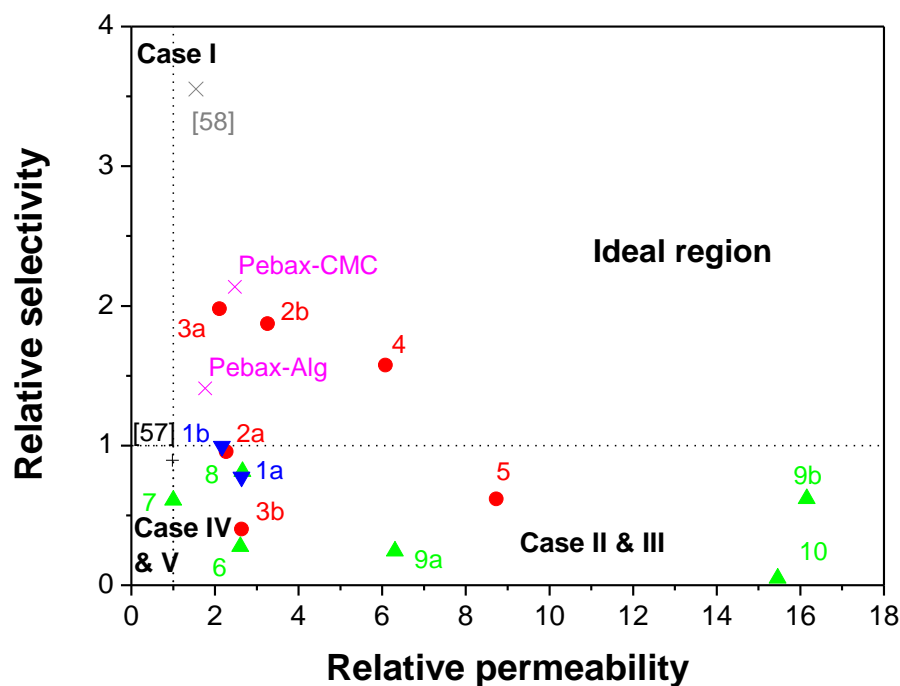


Figure 10. Relative selectivity and permeability of the different POP-filled MMMs in Pebax and CS:PVA matrices as a function of the different morphology cases identified in MMMs. (1a) POP1/Matrimid; (1b) POP-4/Matrimid; (2a) 5% POP1/CS:PVA; (2b) 10 wt% POP-1/CS:PVA; (3a) POP3/CS:PVA; (3b) 10 wt% POP3/CS:PVA; (4) 10 wt% POP4/CS:PVA; (5) 10 wt% POP6/CS:PVA; (6) POP1/Pebax; (7) POP3/Pebax; (8) POP4/Pebax; (9a) 16 wt.% POP6/Pebax; (9b) 32 wt.% POP6/Pebax; (10) POP9/Pebax. Also represented in the figure, CS, swollen [67], CS, TMC [66], Pebax-Alg, and Pebax-CMC [68].

4. Discussion

Comparison of the experimental data with the prediction of Maxwell's ideal model confirmed the presence of non-idealities at the interface of POPs and different polymeric matrices [69].

The CO₂ permeability values of the CS:PVA and Pebax-based MMMs are underestimated by the Maxwell model, these values being closer to the maximum limit determined by the parallel version of Equation (14). In fact, the Matrimid-based MMMs do not converge using Equation (13), which establishes the minimum permeability predicted from

the Maxwell model, probably due to the low permeability values through this polyimide. Another interesting feature observed in these POP-based MMMs that differs from other materials is that the greater the selectivity that the filler material imparts to the heterogeneous MMM, the greater its deviation from the ideal model equation. Figure 10 also highlights that these deviations are more relevant in Pebax-based MMMs, due to the higher porosity of some of the POPs (as in the case of POP9) and a higher amount of filler particle loading (POP6), as observed experimentally. It seems evident that the plasma treatment of the particles was not sufficient to improve the compatibility of polymer and fillers when high-porosity POPs and high polymer network loadings are employed. It is commonly accepted that at high loadings, the Bruggeman model gives a better result, since it approximates the case where the difference in permeability of the dispersed and continuous phases decreases, making $\alpha^* = 1$.

Different phenomenological expressions have been described in the literature to describe the effect of porous organic fillers in MMMs. One of the seminal works was that of Vu et al. [16], in which it was observed that the ideal Maxwell model provided a poor prediction of the observed permeability through MMMs made by Ultem or Matrimid matrices and carbon molecular sieve (CMS) fillers (these materials possess lower permeability values than the Pebax and CS:PVA MMMs prepared in this work). When the predicted permeability is lower than the experimentally obtained permeability, this is generally attributed to particle agglomeration, which causes gas molecules to diffuse preferentially through the particle channels rather than the hypothetical uniform dispersion of the complex MMM system [70] since the ideal Maxwell model does not account for the non-ideal morphologies discussed in Figure 10. Table 7 reflects the mean absolute experimental errors of the CO₂ and CH₄ permeability values predicted by Equations (9), (13) and (14), respectively, where the permeability value through CMS reported in literature is used as a reference for the permeability of the dispersed phase, P_d , in these equations [16]. It can be seen that the gas permeability through the Matrimid-based MMMs is best predicted by the lower bound of the ideal Maxwell model, represented by Equation (13), while the more permeable hydrophilic MMMs based on Pebax and CS:PVA polymers approach the limit represented by Equation (14). The exception to this behavior corresponded to the POP-6-filled MMMs that deviated from the ideal morphology described by the Maxwell model, which can be attributed to the higher porosity afforded by this POP6 to the heterogeneous structure of the MMMs when compared to the other MMMs in this work. These observations agree with data from the literature for other organic cage fillers and PEEK-WC, compared with Matrimid, in MMMs for gas separation [21].

Thus, in this work, modifications of the ideal Maxwell model equation have been evaluated by applying Equation (9) twice, to account for the thickness of the stiffened or empty region between the dispersed porous particle and the continuous polymeric matrix (interface), and the chain immobilization factor that accounts for the decrease in permeability in the vicinity of the particle if stiffening occurs (Cases IV and V in Figure 10) as observed in the literature for CMSs in Matrimid [16]. This modification can be improved to account for the non-ideal pore-blocking behavior that occurs when polymeric chains penetrate porous fillers (Cases II and III in Figure 10), which could explain, in some cases, the increased permeability of the MMM compared to the original pristine polymeric membrane [38]. Thus, Gheimasi et al. included partial pore blocking to predict CO₂/CH₄ separation through CMS-filled MMMs [68]. However, in the modifications of phenomenological MMM transport models applied in carbon molecular sieve-filled MMMs, they only optimized the form factor, n [69], assuming $n = 1/3$ as in Equation (9), as Nasir et al. [70] did to fit their carbon molecular sieve-filled PES MMMs behavior regarding CO₂ separation. Applying Equation (9) twice as a function of two parameters describing the interface/void (interface) distance between the dispersed and continuous phases. For instance, the interface distance values of 0.54 and 1.06 μm , between the POP6 particles and the CS:PVA and Pebax continuous matrices, respectively, and immobilization factors of 0.14 and 0.10, and 0.10 and 0.57, for CO₂ and CH₄, in the CS:PVA and Pebax continuous matrices, respectively,

gave AARE of the gas permeability prediction through the MMMs lower than 0.001%. These values agree with the results obtained previously for ionic liquid/chitosan (IL-CS) MMMs filled with porous ZIF-8 and HKUST-1 nanoparticles [50].

These behavioral observations are attributed to the high CO₂ uptake and differences in the porosity of the POP fillers, with POP6 being larger than the others, and to the dependence of diffusivity on permeability through rigid Matrimid polyimide membranes [21,24], and to the gas solubility that is probably facilitating CO₂ transport through such hydrophilic polymers as Pebax and CS:PVA [28].

5. Conclusions

A new set of mixed matrix membranes was prepared by blending conventional polymers and several porous organic hyper-crosslinked polymers (POPs) as fillers, which were studied in CO₂/CH₄ separation. The employed polymer matrixes were Matrimid and Pebax, and a biopolymer base made from chitosan and polyvinyl alcohol. The gas separation performance was measured in terms of single gas permeability and mixed gas CO₂/CH₂ (50:50 *v/v*%) separation. The compatibility of the POP particles into the polymer matrix was improved by POP plasma treatment before making the blend, for the hydrophilic Pebax and CS:PVA biopolymer. It was observed that the compatibility of the POP particles into the polymer matrices, for the hydrophilic Pebax and CS:PVA biopolymer, was improved by POP plasma treatment before making the blend. The compatibility effect between the porous fillers and matrices onto gas transport was studied by using the Maxwell model as a function of the gas permeability of the pure polymers, the porosity and composition of the fillers, and the composition of the MMMs.

It was observed that the materials could be described by the simple Maxwell model, except in the case of the highly porous POP-derived membranes, where the increased porosity generated non-idealities in the transport mechanism. These anomalous situations should be further explored by considering other issues such as the free volume of the material and the facilitated contribution to the transport mechanism that could occur in the membrane. The performance of bio-based CS.PVA membranes as gas separation membranes approaches the performance of hydrophilic Pebax membranes, which makes these CS.PVA membranes present potential for application in commercial membranes, once the understanding of the influences of the mass transport mechanism is clarified by careful determination of structure-property relationships to accelerate the development of sustainable membranes for different applications by widening the range of materials available for membrane fabrication under criteria within the circular economy.

Author Contributions: Conceptualization, Á.E.L. and C.C.-C.; methodology, C.Á., Á.E.L. and C.C.-C.; validation, L.M.-N., C.Á. and C.C.-C.; formal analysis, L.M.-N., C.Á. and C.C.-C.; investigation, L.M.-N., J.M.-P., C.Á. and C.C.-C.; resources, C.Á., Á.E.L. and C.C.-C.; writing—original draft preparation, L.M.-N., J.M.-P., C.Á., Á.E.L. and C.C.-C.; writing—review and editing, Á.E.L. and C.C.-C.; supervision, C.Á., Á.E.L. and C.C.-C.; project administration, C.Á., Á.E.L. and C.C.-C.; funding acquisition, C.Á., Á.E.L. and C.C.-C. All authors have read and agreed to the published version of the manuscript.

Funding: This research was funded by IVACE program, Generalitat Valenciana, at the University of Cantabria, grant number PRO-81. THE APC was funded by the University of Cantabria. Also, this research was funded by Spain's Agencia Estatal de Investigación (AEI) (Projects: PID2019-109403RB-C22 (AEI/FEDER, UE), and PID2019-109403RB-C21 (AEI/FEDER, UE)).

Institutional Review Board Statement: Not applicable.

Data Availability Statement: Not applicable.

Acknowledgments: Carlos Rodríguez García, John Gómez Rubio, and Andrea Torre Celeizabal are gratefully acknowledged for their experimental contribution to this work, during their final degree, master theses, and Ph.D. thesis at the Universidad de Valladolid, the Instituto de Ciencia y Tecnología de Polímeros (ICTP-CSIC) and the Universidad de Cantabria, respectively.

Conflicts of Interest: The authors declare no conflict of interest. The funders had no role in the design of the study; in the collection, analyses, or interpretation of data; in the writing of the manuscript; or in the decision to publish the results.

References

1. Brémond, U.; Bertrandias, A.; Steyer, J.P.; Bernet, N.; Carrere, H. A Vision of European Biogas Sector Development towards 2030: Trends and Challenges. *J. Clean. Prod.* **2021**, *287*, 125065. [[CrossRef](#)]
2. Tao, J.; Wang, J.; Zhu, L.; Chen, X. Integrated Design of Multi-Stage Membrane Separation for Landfill Gas with Uncertain Feed. *J. Memb. Sci.* **2019**, *590*, 117260. [[CrossRef](#)]
3. Angelidaki, I.; Treu, L.; Tsapekos, P.; Luo, G.; Campanaro, S.; Wenzel, H.; Kougias, P.G. Biogas Upgrading and Utilization: Current Status and Perspectives. *Biotechnol. Adv.* **2018**, *36*, 452–466. [[CrossRef](#)]
4. Torre-Celeizabal, A.; Casado-Coterillo, C.; Abejón, R.; Garea, A. Simultaneous Production of High-Quality CO₂ and CH₄ via Multistage Process Using Chitosan-Based Membranes. *Sep. Purif. Technol.* **2023**, *320*, 124050. [[CrossRef](#)]
5. Evonik Industries. *SEPURAN® Green Membrane Technology for Upgrading Biogas Efficiently*; Evonik Industries: Essen, Germany, 2020.
6. Schuldt, K.; Pohlmann, J.; Shishatskiy, S.; Brinkmann, T. Applicability of Polyactive™ Thin Film Composite Membranes for CO₂ Separation from C₂H₄ Containing Multi-Component Gas Mixtures at Pressures up to 30 Bar. *Membranes* **2018**, *8*, 27. [[CrossRef](#)]
7. Lin, H.; He, Z.; Sun, Z.; Vu, J.; Ng, A.; Mohammed, M.; Kniep, J.; Merkel, T.C.; Wu, T.; Lambrecht, R.C. CO₂-Selective Membranes for Hydrogen Production and CO₂ Capture—Part I: Membrane Development. *J. Memb. Sci.* **2014**, *457*, 149–161. [[CrossRef](#)]
8. Jeon, Y.W.; Lee, D.H. Gas Membranes for CO₂/CH₄ (Biogas) Separation: A Review. *Environ. Eng. Sci.* **2015**, *32*, 71–85. [[CrossRef](#)]
9. Lin, H.; Yavari, M. Upper Bound of Polymeric Membranes for Mixed-Gas CO₂/CH₄ Separations. *J. Memb. Sci.* **2015**, *475*, 101–109. [[CrossRef](#)]
10. Comesaña-Gándara, B.; Chen, J.; Bezzu, C.G.; Carta, M.; Rose, I.; Ferrari, M.C.; Esposito, E.; Fuoco, A.; Jansen, J.C.; McKeown, N.B. Redefining the Robeson Upper Bounds for CO₂/CH₄ and CO₂/N₂ Separations Using a Series of Ultrapermeable Benzotriptycene-Based Polymers of Intrinsic Microporosity. *Energy Environ. Sci.* **2019**, *12*, 2733–2740. [[CrossRef](#)]
11. Powell, C.E.; Qiao, G.G. Polymeric CO₂/N₂ Gas Separation Membranes for the Capture of Carbon Dioxide from Power Plant Flue Gases. *J. Memb. Sci.* **2006**, *279*, 1–49. [[CrossRef](#)]
12. Buonomenna, M.G.; Yave, W.; Golemme, G. Some Approaches for High Performance Polymer Based Membranes for Gas Separation: Block Copolymers, Carbon Molecular Sieves and Mixed Matrix Membranes. *RSC Adv.* **2012**, *2*, 10745–10773. [[CrossRef](#)]
13. Russo, F.; Galiano, F.; Iulianelli, A.; Basile, A.; Figoli, A. Biopolymers for Sustainable Membranes in CO₂ Separation: A Review. *Fuel Process. Technol.* **2021**, *213*, 106643. [[CrossRef](#)]
14. Vatanpour, V.; Yavuzturk Gul, B.; Zeytuncu, B.; Korkut, S.; İlyasoğlu, G.; Turken, T.; Badawi, M.; Koyuncu, I.; Saeb, M.R. Polysaccharides in Fabrication of Membranes: A Review. *Carbohydr. Polym.* **2022**, *281*, 119041. [[CrossRef](#)] [[PubMed](#)]
15. Borgohain, R.; Pattnaik, U.; Prasad, B.; Mandal, B. A Review on Chitosan-Based Membranes for Sustainable CO₂ Separation Applications: Mechanism, Issues, and the Way Forward. *Carbohydr. Polym.* **2021**, *267*, 118178. [[CrossRef](#)] [[PubMed](#)]
16. Chung, T.S.; Jiang, L.Y.; Li, Y.; Kulprathipanja, S. Mixed Matrix Membranes (MMMs) Comprising Organic Polymers with Dispersed Inorganic Fillers for Gas Separation. *Prog. Polym. Sci.* **2007**, *32*, 483–507. [[CrossRef](#)]
17. Xiang, Z.; Cao, D. Porous Covalent-Organic Materials: Synthesis, Clean Energy Application and Design. *J. Mater. Chem. A Mater.* **2013**, *1*, 2691–2718. [[CrossRef](#)]
18. Lopez-Iglesias, B.; Suárez-García, F.; Aguilar-Lugo, C.; González Ortega, A.; Bartolomé, C.; Martínez-Ilarduya, J.M.; De La Campa, J.G.; Lozano, Á.E.; Álvarez, C. Microporous Polymer Networks for Carbon Capture Applications. *ACS Appl. Mater. Interfaces* **2018**, *10*, 26195–26205. [[CrossRef](#)]
19. Venna, S.R.; Carreon, M.A. Metal Organic Framework Membranes for Carbon Dioxide Separation. *Chem. Eng. Sci.* **2015**, *124*, 3–19. [[CrossRef](#)]
20. Shan, M.; Seoane, B.; Andres-Garcia, E.; Kapteijn, F.; Gascon, J. Mixed-Matrix Membranes Containing an Azine-Linked Covalent Organic Framework: Influence of the Polymeric Matrix on Post-Combustion CO₂-Capture. *J. Memb. Sci.* **2018**, *549*, 377–384. [[CrossRef](#)]
21. La Cognata, S.; Mobili, R.; Milanese, C.; Boiocchi, M.; Gaboardi, M.; Armentano, D.; Jansen, J.C.; Monteleone, M.; Antonangelo, A.R.; Carta, M.; et al. CO₂ Separation by Imide/Imine Organic Cages. *Chem. Eur. J.* **2022**, *28*, e202201631. [[CrossRef](#)]
22. Rivera, M.P.; Lively, R.P. Analysis of Gas Transport in Molecularly-Mixed Composite Membranes. *J. Memb. Sci.* **2022**, *661*, 120880. [[CrossRef](#)]
23. Gao, X.; Zou, X.; Ma, H.; Meng, S.; Zhu, G. Highly Selective and Permeable Porous Organic Framework Membrane for CO₂ Capture. *Adv. Mater.* **2014**, *26*, 3644–3648. [[CrossRef](#)]
24. Singh, Z.V.; Tan, L.L.; Cowan, M.G.; Yang, Y.W.; Zhang, W.; Gin, D.L.; Noble, R.D. Pillar [5]Arene/Matrimid™ Materials for High-Performance Methane Purification Membranes. *J. Memb. Sci.* **2017**, *539*, 224–228. [[CrossRef](#)]
25. Wang, Y.; Ren, Y.; Cao, Y.; Liang, X.; He, G.; Ma, H.; Dong, H.; Fang, X.; Pan, F.; Jiang, Z. Engineering HOF-Based Mixed Matrix Membranes for Efficient CO₂ Separation. *Nanomicro Lett.* **2023**, *15*, 50. [[CrossRef](#)]

26. Vinh-Thang, H.; Kaliaguine, S. Predictive Models for Mixed-Matrix Membrane Performance: A Review. *Chem. Rev.* **2013**, *113*, 4980–5028. [[CrossRef](#)]
27. Wang, S.; Liu, Y.; Huang, S.; Wu, H.; Li, Y.; Tian, Z.; Jiang, Z. Pebax-PEG-MWCNT Hybrid Membranes with Enhanced CO₂ Capture Properties. *J. Memb. Sci.* **2014**, *460*, 62–70. [[CrossRef](#)]
28. Rodríguez-Jardón, L.; López-González, M.; Iglesias, M.; Maya, E.M. Effect of Porous Organic Polymers in Gas Separation Properties of Polycarbonate Based Mixed Matrix Membranes. *J. Memb. Sci.* **2021**, *619*, 118795. [[CrossRef](#)]
29. Kanehashi, S.; Aguiar, A.; Lu, H.T.; Chen, G.Q.; Kentish, S.E. Effects of Industrial Gas Impurities on the Performance of Mixed Matrix Membranes. *J. Memb. Sci.* **2018**, *549*, 686–692. [[CrossRef](#)]
30. Minelli, M.; Doghieri, F.; Papadokostaki, K.G.; Petropoulos, J.H. A Fundamental Study of the Extent of Meaningful Application of Maxwell's and Wiener's Equations to the Permeability of Binary Composite Materials. Part I: A Numerical Computation Approach. *Chem. Eng. Sci.* **2013**, *104*, 630–637. [[CrossRef](#)]
31. Vu, D.Q.; Koros, W.J.; Miller, S.J. Mixed Matrix Membranes Using Carbon Molecular Sieves: II. Modeling Permeation Behavior. *J. Memb. Sci.* **2003**, *211*, 335–348. [[CrossRef](#)]
32. Klepić, M.; Fuoco, A.; Monteleone, M.; Esposito, E.; Friess, K.; Izák, P.; Jansen, J.C. Effect of the CO₂-Philic Ionic Liquid [BMIM][Tf₂N] on the Single and Mixed Gas Transport in PolyActive™ Membranes. *Sep. Purif. Technol.* **2021**, *256*, 117813. [[CrossRef](#)]
33. Rahman, M.M.; Filiz, V.; Shishatskiy, S.; Abetz, C.; Georgopoulos, P.; Khan, M.M.; Neumann, S.; Abetz, V. Influence of Poly(Ethylene Glycol) Segment Length on CO₂ Permeation and Stability of Polyactive Membranes and Their Nanocomposites with PEG POSS. *ACS Appl. Mater. Interfaces* **2015**, *7*, 12289–12298. [[CrossRef](#)] [[PubMed](#)]
34. Galiano, F.; Briceño, K.; Marino, T.; Molino, A.; Christensen, K.V.; Figoli, A. Advances in Biopolymer-Based Membrane Preparation and Applications. *J. Memb. Sci.* **2018**, *564*, 562–586. [[CrossRef](#)]
35. Tomietto, P.; Russo, F.; Galiano, F.; Loulergue, P.; Salerno, S.; Paugam, L.; Audic, J.L.; De Bartolo, L.; Figoli, A. Sustainable Fabrication and Pervaporation Application of Bio-Based Membranes: Combining a Polyhydroxyalkanoate (PHA) as Biopolymer and Cyrene™ as Green Solvent. *J. Memb. Sci.* **2022**, *643*, 120061. [[CrossRef](#)]
36. Gao, J.; Zhu, C.; Zhu, M.; Fu, Y.; Huang, H.; Liu, Y.; Kang, Z. Highly Selective and Efficient Electroreduction of Carbon Dioxide to Carbon Monoxide with Phosphate Silver-Derived Coral-like Silver. *ACS Sustain. Chem. Eng.* **2019**, *7*, 3536–3543. [[CrossRef](#)]
37. Rico-Martínez, S.; Álvarez, C.; Hernández, A.; Miguel, J.A.; Lozano, Á.E. Mixed Matrix Membranes Loaded with a Porous Organic Polymer Having Bipyridine Moieties. *Membranes* **2022**, *12*, 547. [[CrossRef](#)] [[PubMed](#)]
38. Hashemifard, S.A.; Ismail, A.F.; Matsuura, T. A New Theoretical Gas Permeability Model Using Resistance Modeling for Mixed Matrix Membrane Systems. *J. Memb. Sci.* **2010**, *350*, 259–268. [[CrossRef](#)]
39. Wang, Y.; Goh, S.H.; Chung, T.S. Miscibility Study of Torlon® Polyamide-Imide with Matrimid® 5218 Polyimide and Polybenzimidazole. *Polymer* **2007**, *48*, 2901–2909. [[CrossRef](#)]
40. Boroglu, M.-S.; Ugur, M.; Boz, I. Enhanced Gas Transport Properties of Mixed Matrix Membranes Consisting of Matrimid and RHO Type ZIF-12 Particles. *Chem. Eng. Res. Des.* **2017**, *123*, 201–213. [[CrossRef](#)]
41. Sakurai, K.; Maegawa, T.; Takahashi, T. Glass Transition Temperature of Chitosan and Miscibility of Chitosan/Poly(N-Vinyl Pyrrolidone) Blends. *Polymer* **2000**, *41*, 7051–7056. [[CrossRef](#)]
42. Chung, T.S.; Chan, S.S.; Wang, R.; Lu, Z.; He, C. Characterization of Permeability and Sorption in Matrimid/C60 Mixed Matrix Membranes. *J. Memb. Sci.* **2003**, *211*, 91–99. [[CrossRef](#)]
43. Mi, F.L.; Shyu, S.S.; Wu, Y.B.; Lee, S.T.; Shyong, J.Y.; Huang, R.N. Fabrication and Characterization of a Sponge-like Asymmetric Chitosan Membrane as a Wound Dressing. *Biomaterials* **2001**, *22*, 165–173. [[CrossRef](#)] [[PubMed](#)]
44. Song, R.; Xue, R.; He, L.; Liu, Y.; Xiao, Q. The Structure and Properties of Chitosan/Polyethylene Glycol/Silica Ternary Hybrid Organic-Inorganic Films. *Chin. J. Polym. Sci.* **2008**, *26*, 621–630. [[CrossRef](#)]
45. Chen, G.Q.; Scholes, C.A.; Doherty, C.M.; Hill, A.J.; Qiao, G.G.; Kentish, S.E. The Thickness Dependence of Matrimid Films in Water Vapor Permeation. *Chem. Eng. J.* **2012**, *209*, 301–312. [[CrossRef](#)]
46. Pardo, F.; Zarca, G.; Urriaga, A. Separation of Refrigerant Gas Mixtures Containing R32, R134a, and R1234yf through Poly(Ether-Block-Amide) Membranes. *ACS Sustain. Chem. Eng.* **2020**, *8*, 2548–2556. [[CrossRef](#)]
47. Casado-Coterillo, C.; del Mar López-Guerrero, M.; Irabien, Á. Synthesis and Characterisation of ETS-10/Acetate-Based Ionic Liquid/Chitosan Mixed Matrix Membranes for CO₂/N₂ Permeation. *Membranes* **2014**, *4*, 287–301. [[CrossRef](#)]
48. Marcos-Madrado, A.; Casado-Coterillo, C.; García-Cruz, L.; Iniesta, J.; Simonelli, L.; Sebastián, V.; Encabo-Berzosa, M.d.M.; Arruebo, M.; Irabien, Á. Preparation and Identification of Optimal Synthesis Conditions for a Novel Alkaline Anion-Exchange Membrane. *Polymers* **2018**, *10*, 913–922. [[CrossRef](#)]
49. Santos, E.; Rodríguez-Fernández, E.; Casado-Coterillo, C.; Irabien, Á. Hybrid Ionic Liquid-Chitosan Membranes for CO₂ Separation: Mechanical and Thermal Behavior. *Int. J. Chem. React. Eng.* **2016**, *14*, 713–718. [[CrossRef](#)]
50. Casado-Coterillo, C.; Fernández-Barquín, A.; Zornoza, B.; Téllez, C.; Coronas, J.; Irabien, Á. Synthesis and Characterisation of MOF/Ionic Liquid/Chitosan Mixed Matrix Membranes for CO₂/N₂ Separation. *RSC Adv.* **2015**, *5*, 102350–102361. [[CrossRef](#)]
51. Abarca, J.A.; Díaz-Sainz, G.; Merino-García, I.; Beobide, G.; Albo, J.; Irabien, A. Optimized Manufacturing of Gas Diffusion Electrodes for CO₂ Electroreduction with Automatic Spray Pyrolysis. *J. Environ. Chem. Eng.* **2023**, *11*, 109724. [[CrossRef](#)]
52. Franck-Lacaze, L.; Sístat, P.; Huguet, P. Determination of the PKa of Poly (4-Vinylpyridine)-Based Weak Anion Exchange Membranes for the Investigation of the Side Proton Leakage. *J. Memb. Sci.* **2009**, *326*, 650–658. [[CrossRef](#)]

53. Wijmans, J.G.; Baker, R.W. The Solution-Diffusion Model: A Review. *J. Memb. Sci.* **1995**, *107*, 1–21. [[CrossRef](#)]
54. Torre-Celeizabal, A.; Casado-Coterillo, C.; Garea, A. Biopolymer-Based Mixed Matrix Membranes (MMMs) for CO₂/CH₄ Separation: Experimental and Modeling Evaluation. *Membranes* **2022**, *12*, 561–583. [[CrossRef](#)] [[PubMed](#)]
55. Kanehashi, S.; Chen, G.Q.; Scholes, C.A.; Ozcelik, B.; Hua, C.; Ciddor, L.; Southon, P.D.; D’Alessandro, D.M.; Kentish, S.E. Enhancing Gas Permeability in Mixed Matrix Membranes through Tuning the Nanoparticle Properties. *J. Memb. Sci.* **2015**, *482*, 49–55. [[CrossRef](#)]
56. Hua, C.; Rawal, A.; Faust, T.B.; Southon, P.D.; Babarao, R.; Hook, J.M.; D’Alessandro, D.M. Exploiting Stable Radical States for Multifunctional Properties in Triarylamine-Based Porous Organic Polymers. *J. Mater. Chem. A Mater.* **2014**, *2*, 12466–12474. [[CrossRef](#)]
57. El-Azzami, L.A.; Grulke, E.A. Parametric Study of CO₂ Fixed Carrier Facilitated Transport through Swollen Chitosan Membranes. *Ind. Eng. Chem. Res.* **2009**, *48*, 894–902. [[CrossRef](#)]
58. Dhawade, P.P.; Jagtap, R.N. Characterization of the Glass Transition Temperature of Chitosan and Its Oligomers by Temperature Modulated Differential Scanning Calorimetry. *Pelagia Res. Libr. Adv. Appl. Sci. Res.* **2012**, *3*, 1372–1382.
59. Dai, Y.; Ruan, X.; Yan, Z.; Yang, K.; Yu, M.; Li, H.; Zhao, W.; He, G. Imidazole Functionalized Graphene Oxide/PEBAX Mixed Matrix Membranes for Efficient CO₂ Capture. *Sep. Purif. Technol.* **2016**, *166*, 171–180. [[CrossRef](#)]
60. Kanehashi, S.; Chen, G.Q.; Danaci, D.; Webley, P.A.; Kentish, S.E. Can the Addition of Carbon Nanoparticles to a Polyimide Membrane Reduce Plasticization? *Sep. Purif. Technol.* **2017**, *183*, 333–340. [[CrossRef](#)]
61. Tan, P.C.; Jawad, Z.A.; Ooi, B.S.; Ahmad, A.L.; Low, S.C. Correlation between Polymer Packing and Gas Transport Properties for CO₂/N₂ Separation in Glassy Fluorinated Polyimide Membrane. *J. Eng. Sci. Technol.* **2016**, *11*, 935–946.
62. Robeson, L.M. Correlation of Separation Factor versus Permeability for Polymeric Membranes. *J. Memb. Sci.* **1991**, *62*, 165–185. [[CrossRef](#)]
63. Robeson, L.M. The Upper Bound Revisited. *J. Memb. Sci.* **2008**, *320*, 390–400. [[CrossRef](#)]
64. Luna, A.D.; de León, G.C.; Rodríguez, S.P.; López, N.C.; Camacho, O.P.; Mercado, Y.A. Na⁺/Ca²⁺ Aqueous Ion Exchange in Natural Clinoptilolite Zeolite for Polymer-Zeolite Composite Membranes Production and Their CH₄/CO₂/N₂ Separation Performance. *J. Nat. Gas. Sci. Eng.* **2018**, *54*, 47–53. [[CrossRef](#)]
65. Minelli, M.; Sarti, G.C. Permeability and Diffusivity of CO₂ in Glassy Polymers with and without Plasticization. *J. Memb. Sci.* **2013**, *435*, 176–185. [[CrossRef](#)]
66. Xiao, S.; Feng, X.; Huang, R.Y.M. Trimesoyl Chloride Crosslinked Chitosan Membranes for CO₂/N₂ Separation and Pervaporation Dehydration of Isopropanol. *J. Memb. Sci.* **2007**, *306*, 36–46. [[CrossRef](#)]
67. Ito, A.; Sato, M.; Anma, T. Permeability of CO₂ through Chitosan Membrane Swollen by Water Vapor in Feed Gas. *Angew. Makromol. Chem.* **1997**, *248*, 85–94. [[CrossRef](#)]
68. Salestan, S.K.; Rahimpour, A.; Abedini, R. Experimental and Theoretical Studies of Biopolymers on the Efficient CO₂/CH₄ Separation of Thin-Film Pebax[®]1657 Membrane. *Chem. Eng. Process.-Process Intensif.* **2021**, *163*, 108366. [[CrossRef](#)]
69. Casado-Coterillo, C.; Fernández-Barquín, A.; Valencia, S.; Irabien, Á. Estimating CO₂/N₂ Permselectivity through Si/Al = 5 Small-Pore Zeolites/PTMSP Mixed Matrix Membranes: Influence of Temperature and Topology. *Membranes* **2018**, *8*, 32. [[CrossRef](#)]
70. Hao, L.; Li, P.; Yang, T.; Chung, T.S. Room Temperature Ionic Liquid/ZIF-8 Mixed-Matrix Membranes for Natural Gas Sweetening and Post-Combustion CO₂ Capture. *J. Memb. Sci.* **2013**, *436*, 221–231. [[CrossRef](#)]

Disclaimer/Publisher’s Note: The statements, opinions and data contained in all publications are solely those of the individual author(s) and contributor(s) and not of MDPI and/or the editor(s). MDPI and/or the editor(s) disclaim responsibility for any injury to people or property resulting from any ideas, methods, instructions or products referred to in the content.